HHS Public Access

Author manuscript

*Opt Lett*. Author manuscript; available in PMC 2019 May 29.

Published in final edited form as:

*Opt Lett*. 2019 May 01; 44(9): 2232–2235. doi:10.1364/OL.44.002232.

# Ultralow-voltage electrothermal MEMS based fiber-optic scanning probe for forward-viewing endoscopic OCT

**Hyeon-Cheol Park**[1], **Xiaoyang Zhang**[2], **Wu Yuan**[1], **Liang Zhou**[2], **Huikai Xie**[2], and **Xingde Li**[1,*]

[1]Department of Biomedical Engineering, School of Medicine, Johns Hopkins University, Baltimore, Maryland 21205, USA

[2]Department of Electrical and Computer Engineering, University of Florida, Gainesville, Florida 32611, USA

## Abstract

We report an ultralow-voltage, electrothermal (ET) microelectro-mechanical system (MEMS) based probe for forward-viewing endoscopic optical coherence tomography (OCT) imaging. The fully assembled probe has a diameter of 5.5 mm and a length of 55 mm, including the imaging optics and a 40 mm long fiber-optic cantilever attached on a micro-platform of the bimorph ET MEMS actuator. The ET MEMS actuator provides a sufficient mechanical actuation force as well as a large vertical displacement, achieving up to a 3 mm optical scanning range with only a 3 $V_{ACp–p}$ drive voltage with a 1.5 $V_{DC}$ offset. The imaging probe was integrated with a swept-source OCT system of a 100 kHz A-scan rate, and its performance was successfully demonstrated with cross-sectional imaging of biological tissues *ex vivo* and *in vivo* at a speed up to 200 frames per second.

Optical coherence tomography (OCT) is a medical imaging modality that can provide cross-sectional images of biological tissue with microscopic resolution and a few millimeters of imaging depth non-invasively and in real time [1]. OCT can be a powerful diagnostic tool especially for detecting early stage diseases developing from the superficial linings of internal organs [2]. Translating OCT for internal organ imaging requires a scanning endoscope/laparoscope. Recent development of endoscopic OCT technologies successfully demonstrated the capability of OCT for detecting diseases in the gastrointestinal tract such as Barrett's esophagus [3], ulcerative colitis [4], and inflammatory bowel disease [5]. Potential applications in various other organs have also been actively investigated, such as the respiratory tract [6] and pancreas [7].

For decades, various types of endoscopic catheters or probes have been developed. Particularly circumferential scanning endoscopes, either with the entire endoscope rotated with an external rotary joint at the proximal end [8,9] or with a beam reflector rotated with a micromotor at the distal end [10], have been developed, and some have already been translated into clinical trials or approved practices [11]. While circumferential scanning endoscopes are suitable for surveying a large area along luminal organs, forward-viewing

*Corresponding author: xingde@jhu.edu.

endoscopes are more desirable for image-guided biopsy or surgery. However, forward beam scanning inside a miniature probe with limited space is challenging. It requires a miniaturized scanner and often requires additional beam-folding optics to deflect the beam towards forward direction. A few forward-viewing probes have been demonstrated by scanning a fiber [12–20], rotating a pair of angled lenses [21], or by scanning a MEMS-lens [22]. Among those, the fiber-optic scanner has attractive advantages due to its relatively compact and simple configuration. In particular, a fiber-optic scanner with a tubular piezoelectric (PZT) actuator has been demonstrated for OCT [12–14], multi-photon [15–18], and confocal endoscopy [19]. A cantilevered optical fiber was attached to the distal end of a PZT tube and resonantly scanned with either a spiral [12,14,15,18] or Lissajous [13,17,20] pattern. A few non-resonant fiber-optic scanners based on a piezo bender actuator [16] or an electro-magnetic actuator [19] have been reported but require a high operating voltage up to 200 V, which is an electrical safety concern for clinical applications.

Here we report an ultralow voltage electrothermal (ET) MEMS based fiber-optic scanning probe for forward-viewing endoscopic OCT imaging. An ET bimorph MEMS actuator was used to drive a fiber cantilever and allows forward beam scanning by a piston motion (out-of-plane). The ET actuation offers a sufficient force, enables an ultralow voltage operation of a MEMS scanner, and realizes both resonant and non-resonant scanning of a fiber cantilever over a millimeter range, making it possible to perform raster beam scanning. The performance of this new ET MEMS based fiber-optic scanning probe was demonstrated by imaging biological tissues in real time along with a swept-source OCT (SS-OCT) system.

Figures 1A and 1B show the schematics of the fiber scanning mechanism with the ET MEMS scanner and the probe assembly. A cantilevered fiber was mounted on the top of the micro-platform of an ET MEMS scanner, and optical beam scanning was realized by moving the fiber with the MEMS scanner along the vertical direction (indicated by the red double-ended arrows). Figures 1C and 1D show SEM images of the ET MEMS scanner, which was composed of a micro-platform, supported by two pairs of connecting frames with a three-segmented bimorph actuator [23]. Each bimorph actuator consisted of a top aluminum (Al) layer and a bottom silicon dioxide ($SiO_2$) layer, which had a large difference in the coefficient of thermal expansion (CTE). A platinum (Pt) layer was sandwiched between the two layers as a Joule heating layer (Fig. 1D). When a voltage was applied between a pair of three-segmented bimorph actuators, a current flowed along the Pt layer and the temperature of the bimorph actuators would be increased by Joule heating (Fig. 1C). As the temperature increased, each bimorph segment would bend downward as the higher CTE layer, i.e., the Al layer, was on the top. Consequently, the micro-platform would be lowered down. The supporting frames with a three-segmented bimorph actuator was specifically designed to obtain a pure and efficient vertical (out-of-plane) motion of the micro-platform. Each frame rotates in the opposite direction, which cancels out the lateral shift during bending. The resistances of the two pairs of the three-segmented bimorph actuators were measured to be 44 ohm and 74 ohm, respectively. This mismatch in resistance could arise from microfabrication tolerances, contact resistances, and/or non-uniform wiring during the assembling process. An additional resistor was added outside of the probe in order to compensate the resistance mismatch and obtain a pure vertical motion.

The ET MEMS based fiber-optic scanning probe consisted of three parts: an ET MEMS scanner assembly with a 3D printed base, a fiber assembly, and an optics assembly. These three parts were separately assembled and encased inside a hypodermic tube with a ~5.5 mm outer diameter. Precision optical alignment between the fiber and the focusing optics was crucial during probe assembly. Also, the fiber cantilever needed to be carefully placed along the center line of the micro-platform of the MEMS scanner in order to avoid potential imbalance of the force applied by each bimorph actuator during scanning. Custom designed auxiliary structures, such as spacers and mating sleeves, were used between each assembly component in order to ensure precise separation between adjacent components as well as optical axis alignment. For example, the outer and inner diameters of the mating sleeves should match with the inner diameter of the housing hypodermic tube and the outer diameter of the spacers, respectively, in order to center all the components along the probe longitudinal direction. This modular procedure enabled much efficient assembly with minimal manual adjustment. Figures 1E and 1F show the photos of the probe assembly components. For the assembly procedure, at first, the MEMS scanner was mounted on a 3D printed base, which comprised wire/fiber grooves and a MEMS scanner mounting groove to assist assembling (see Fig. 1B inset). Then, drive wires were directly soldered on the device without any printed circuit board. Second, for the fiber assembly, an optical fiber was first inserted into a ceramic ferrule of a 1.25 mm outer diameter. A 40 mm long fiber was then cantilevered from the ceramic ferrule with epoxy, and the center of the fiber cantilever was positioned on the top of the micro-platform of the ET MEMS scanner (20 mm away from the fixed end). During assembling, a small DC voltage was applied to the MEMS actuator to lower the initial position of the micro-platform for ease fiber mounting. The imaging optic assembly consisted of two commercially available achromatic lenses of a 3 mm diameter. The beam from the fiber was collimated by the first lens ($f_1$ = 3 mm) and then focused by the second lens ($f_2$ = 9 mm). This conventional telescope configuration provided a theoretical 3X magnification and an ~14 μm lateral resolution in the focal plane. Finally, the MEMS scanner along with a base, the fiber assembly, and the optics assembly were integrated inside a hypodermic tube. Figure 1G shows a photograph of the fully assembled probe. The overall rigid length of the probe was 55 mm.

The beam scanning performance of the assembled ET MEMS fiber-optic probe was first investigated before imaging studies. Figure 2A shows the frequency response of the ET MEMS scanner. The ET MEMS fiber-optic scanner can be modeled as a cantilever supported by the MEMS actuator, which in turn can be modeled as a spring. The resonant frequency of the scanner is then mainly determined by the overall cantilever length and the location of the MEMS actuator under the cantilever. In brief, a shorter cantilever length, or a location of the MEMS actuator further from the fixed end provides higher resonant frequency. Then, the cantilevered fiber length and the MEMS actuator location can be chosen to have a resonant frequency that matches the sweeping speed of the OCT light source and produce a given imaging frame rate. For example, with a 40 mm fiber length and the MEMS scanner positioned 20 mm away from the fixed end (the ferrule), as shown in Fig. 1A, the resonant frequency was measured to be ~100 Hz with a Q-factor of ~28. Detailed information about the scanner design can also be found elsewhere [24]. At the resonance, a 3 mm beam scanning range was achieved with an ultralow peak-to-peak

actuation voltage of about 3 $V_{AC}$ with a 1.5 $V_{DC}$ bias (i.e., $V_{in} = 1.5 + 1.5 \sin(\omega t)$), as shown in the inset photograph of Fig. 2A.

The sufficiently large actuation force generated by the ET MEMS scanner enabled not only resonant but also non-resonant scanning of the fiber cantilever. Figure 2B shows the displacement of a fiber tip when a DC voltage was applied to the scanner. A fiber tip displacement greater than 1 mm could be readily achieved with an ultralow actuation voltage of only 2 $V_{DC}$, which is 2 orders of magnitude lower voltage than previously reported non-resonant scanners [16,19].

The imaging performance of the ET MEMS fiber-optic probe was demonstrated with an SS-OCT system. Figure 3 illustrates the schematic of the SS-OCT system, which consisted of a vertical-cavity surface-emitting laser (VCSEL) swept light source (Axsun Technologies). The VCSEL provided a 100 kHz A-line scan rate at a central wavelength of 1310 nm and a 3 dB spectral bandwidth of approximately 88 nm (and a 10 dB bandwidth of ~130 nm).

The laser was divided into the sample and reference arms with a 90/10 fiber-optic coupler, and the OCT interference signal was collected by a balanced detector. The VCSEL source offered an internal linear *k* clock (with an imaging depth up to 6 mm in air), which was used to trigger a high-speed DAQ card (AlazarTech) for synchronized data acquisition. An aiming green laser (532 nm) was coupled into a sample arm with a fiber-optic wavelength division multiplexer (WDM, Thorlabs). The axial resolution of the system was measured to be approximately 9 μm (in air) at an imaging depth of 1.5 mm, while the detection sensitivity and the signal roll-off were measured to be over −115 dB (with a 9.2 mW incident power on the sample) and −0.06 dB/mm, respectively. For OCT imaging, the MEMS probe was driven at its resonant frequency of 100 Hz, with an ultralow peak-to-peak voltage of 3 $V_{AC}$ and a bias of 1.5 $V_{DC}$. The probe could achieve a 3 mm beam scanning range at the focal plane located at 9 mm in front of the probe and equal to its working distance. Due to the limited aperture and off-axis aberrations of the small diameter objective lenses, the image plane was changed by ~0.4 mm at the maximum scan range. However, we were still able to obtain diffraction-limited imaging performances with a measured lateral resolution of ~17 μm. The OCT imaging frame rate was determined by the driving frequency of the MEMS-based fiber-optic scanner and the number of A-lines per frame for a given wavelength sweeping rate of the light source. For example, in our particular experiments, we could choose either 100 frames per second (fps) for unidirectional imaging or 200 fps for bidirectional imaging by adjusting the number of A-lines per image frame. It is noted that the resonant operation of the fiber cantilever induces a phase delay between the MEMS scanner motion and the fiber tip motion ($\pi/2$ radian at resonance), and this phase delay was compensated by carefully tuning the time delay between the probe drive waveform and the time window for OCT signal acquisition. For OCT image reconstruction, about 80% of the scanning range was linearly resampled, considering non-uniform (sinusoidal) scanning speed of the ET MEMS scanner. Figures 4A–4C show representative *in vivo* cross-sectional OCT images of human nail fold, fingerprints, and an *ex vivo* rat intestine sample captured with the ET MEMS scanning probe in real time. Layered structures underneath the surface, such as the nail plate, cuticle, stratum corneum, stratum spinosum, as well as sweat duct were appreciated in Figs. 4A and 4B. Tissue layers, such as mucosa, submucosa, and muscularis

propria were also identified in Fig. 4C. For the images presented in Fig. 4, the frame rate was adjusted to 100 fps and 800 A-lines were captured to reconstruct each OCT image.

To conclude, we developed and demonstrated a new type of forward-viewing OCT imaging probe based on an ET MEMS fiber-optic scanner. The probe was integrated with an SS-OCT system, and real time imaging of biological tissues *ex vivo* and *in vivo* was performed to demonstrate the performance of the probe. The ET MEMS scanner provided a sufficiently large force and enabled an ultralow (i.e., 3 $V_{ACp-p}$ + 1.5 $V_{DC}$) voltage operation at the resonance and non-resonance of the fiber-optic cantilever. This unique advantage of the ET actuation allows for step-wise linear beam scanning as well as fast resonant beam scanning and can offer potential versatility in choosing a beam scanning pattern. Moreover, two-dimensional raster scanning can also be conveniently realized by adding another in-plane actuator. The current probe has an outer diameter of 5.5 mm due to the large footprint of the MEMS scanner of 3 mm (at ~1 mm apart from the probe center). Further miniaturization of the probe can be realized by reducing the MEMS scanner size with advanced designs. The reported ET MEMS imaging probe can potentially provide an alternative avenue for developing forward-viewing miniature OCT probes, such as miniature hand-held probes or laparoscopic probes.

## Acknowledgments

**Funding.** National Institutes of Health (NIH) (R01CA153023, R01CA200399, R01EB020601).

## REFERENCES

1. Tearney GJ, Brezinski ME, Bouma BE, Boppart SA, Pitris C, Southern JF, and Fujimoto JG, Science 276, 2037 (1997). [PubMed: 9197265]
2. Gora MJ, Suter MJ, Tearney GJ, and Li XD, Biomed. Opt. Express 8, 2405 (2017). [PubMed: 28663882]
3. Bouma BE, Tearney GJ, Compton CC, and Nishioka NS, Gastrointest. Endosc 51, 467 (2000). [PubMed: 10744824]
4. Adler DC, Zhou C, Tsai T-H, Schmitt J, Huang Q, Mashimo H, and Fujimoto JG, Opt. Express 17, 784 (2009). [PubMed: 19158891]
5. Consolo P, Strangio G, Luigiano C, Giacobbe G, Pallio S, and Familiari L, Dis. Colon Rectum 51, 1374 (2008). [PubMed: 18546041]
6. Adams DC, Hariri LP, Miller AJ, Wang Y, Cho JL, Villiger M, Holz JA, Szabari MV, Hamilos DL, Harris RS, Griffith JW, Bouma BE, Luster AD, Medoff BD, and Suter MJ, Sci. Transl. Med 8, 359 (2016).
7. Hwang JH, Cobb MJ, Kimmey MB, and Li XD, Clin. Gastroenterol. Hepatol 3, S49 (2005). [PubMed: 16012997]
8. Yuan W, Brown R, Mitzner W, Yarmus L, and Li XD, Nat. Commun. 8, 1531 (2017). [PubMed: 29142274]
9. Park H-C, Mavadia-Shukla J, Yuan W, Alemohammad M, and Li XD, Opt. Lett 42, 4978 (2017). [PubMed: 29216160]
10. Liang K, Traverso G, Lee H-C, Ahsen OO, Wang Z, Potsaid B, Giacomelli M, Jayaraman V, Barman R, Cable A, Mashimo H, Langer R, and Fujimoto JG, Biomed. Opt. Express 6, 1146 (2015). [PubMed: 25909001]
11. Gora MJ, Sauk JS, Carruth RW, Gallagher KA, Suter MJ, Nishioka NS, Kava LE, Rosenberg M, Bouma BE, and Tearney GJ, Nat. Med 19, 238 (2013). [PubMed: 23314056]

12. Liu X, Cobb MJ, Chen Y, Kimmey MB, and Li XD, Opt. Lett 29, 1763 (2004). [PubMed: 15352362]
13. Park H-C, Seo Y-H, Hwang K, Lim J-K, Yoon SZ, and Jeong K-H, Opt. Lett 39, 6675 (2014). [PubMed: 25490650]
14. Schulz-Hildebrandt H, Pfeiffer T, Eixmann T, Lohmann S, Ahrens M, Rehra J, Draxinger W, König P, Huber R, and Hüttmann G, Opt. Lett 43, 4386 (2018). [PubMed: 30211870]
15. Myaing MT, MacDonald DJ, and Li XD, Opt. Lett 31, 1076 (2006). [PubMed: 16625908]
16. Rivera D, Brown C, Ouzounov D, Pavlova I, Kobat D, Webb W, and Xu C, Proc. Natl. Acad. Sci. USA 108, 17598 (2011). [PubMed: 22006303]
17. Liang W, Murari K, Zhang YY, Chen Y, Li XD, and Li M-J, J. Biomed. Opt 17, 021108 (2012). [PubMed: 22463026]
18. Liang W, Hall G, Messerschmidt B, Li M-J, and Li XD, Light Sci. Appl 6, e17082 (2017). [PubMed: 29854567]
19. Hendriks BHW, Bierhoff WCJ, Horikx JJL, Desjardins AE, Hezemans CA, t'Hooft GW, Lucassen GW, and Mihajlovic N, J. Biomed. Opt 16, 026007 (2011). [PubMed: 21361691]
20. Seo Y-H, Hwang K, Park H-C, and Jeong K-H, Opt. Express 24, 3903 (2016). [PubMed: 26907043]
21. Wu J, Conry M, Gu C, Wang F, Yaqoob Z, and Yang C, Opt. Lett 31, 1265 (2006). [PubMed: 16642080]
22. Park H-C, Song C, Kang M, Jeong Y, and Jeong K-H, Opt. Lett 37, 2673 (2012). [PubMed: 22743491]
23. Wu L and Xie H, Sens. Actuators A Phys 145, 371 (2008).
24. Zhang X, Duan C, Liu L, Li XD, and Xie H, Sens. Actuators A Phys 233, 239 (2015). [PubMed: 26347583]

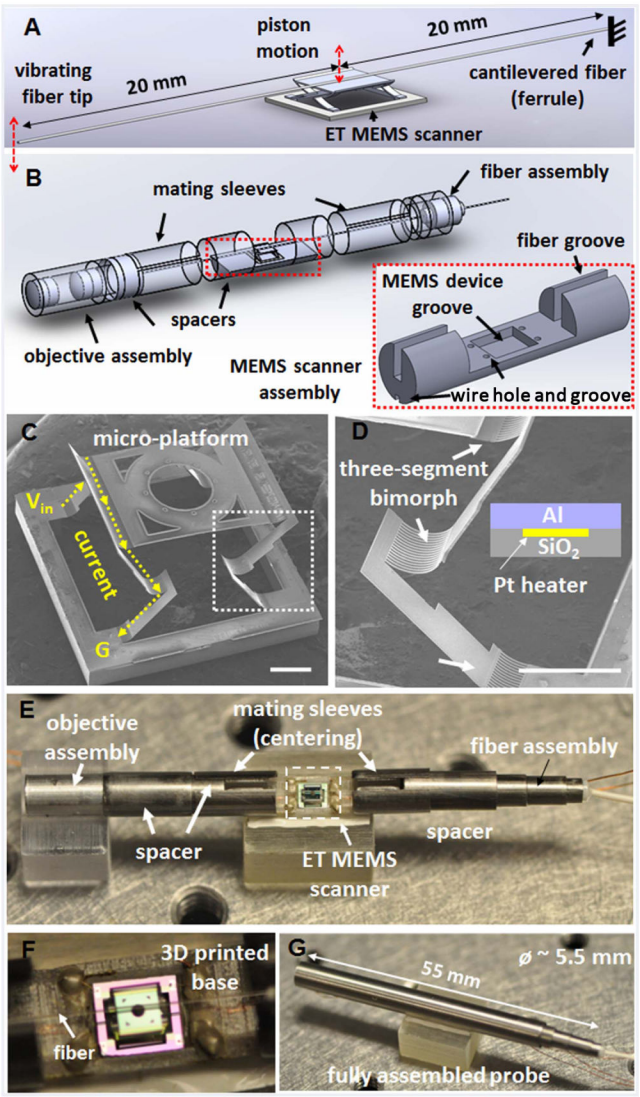


**Fig. 1.**

Schematics of (A) the fiber scanning mechanism and (B) the probe assembly, consisting of an ET MEMS actuator. (C), (D) SEM images of an integrated ET MEMS bimorph actuator; a micro-platform is supported and actuated by two pairs of three-segmented bimorph actuators with two connecting frames, which enable pure vertical motion with a large scanning amplitude. Scale bar: 500 μm. (D) Enlarged view of a three-segmented bimorph actuator [white boxed area in (C)]. ET bimorph actuator is composed of an Al, $SiO_2$, and Pt layer. The Pt layer was sandwiched between the other two layers as a heating layer. Scale bar: 500 μm. (E) Photograph of the probe assembly; a 40 mm long fiber cantilever was mounted on top of the micro-platform of the ET MEMS scanner. (F) Magnified view showing the fiber was aligned with the center line of the ET MEMS scanner along the probe longitudinal axis. (G) Photograph of a fully integrated probe. Objective lenses and the fiber scanner were assembled with holders placed inside a hypodermic tube of a ~5.5 mm outer diameter and a 55 mm overall rigid length.

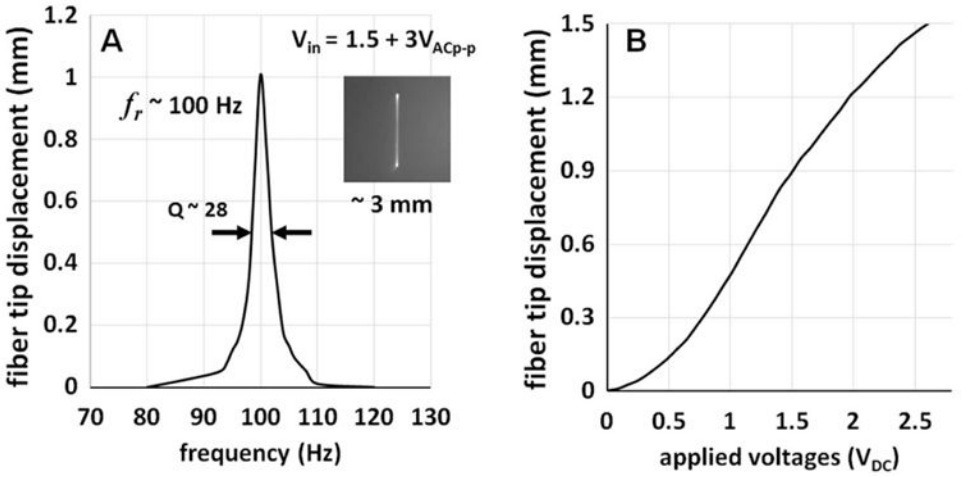


**Fig. 2.**

(A) Frequency response of the ET MEMS fiber-optic scanner. Resonant frequency of the scanner was measured to ~100 Hz and a 3 mm beam scanning range was achieved with a drive voltage of only 3 $V_{ACp-p}$ on top of a 1.5 $V_{DC}$ bias. The inset in (A) shows a photograph of the resonant beam scanning line in the focal plane. (B) Static displacement of the fiber cantilever tip with respect to the drive DC voltages. A relatively large actuation force of the ET bimorph actuator allows for a more than 1 mm fiber tip scanning range with a less than 2 $V_{DC}$ drive voltage.

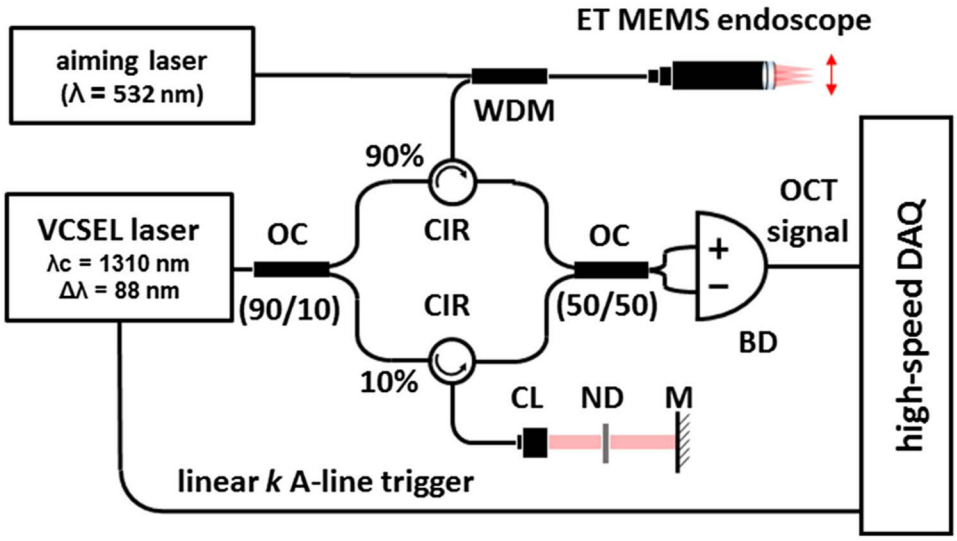


**Fig. 3.**

Schematic of a SS-OCT system integrated with the ET MEMS based scanning probe. A VCSEL with a 100 kHz A-line scan rate was used as the light source. A linear *k* clock generated by the VCSEL was used as the A-line trigger for OCT data acquisition. An aiming laser at 532 nm was coupled into the sample arm with a fiber-optic WDM. OC, fiber-optic coupler; CIR, fiber-optic circulator; WDM, wavelength division multiplexer; BD, balanced detector; CL, collimating lens; ND, neutral density filter; M, mirror.

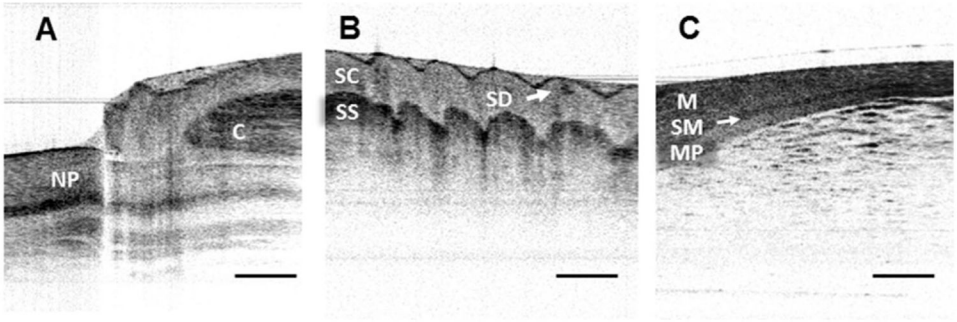


**Fig. 4.**

Representative OCT images captured with the ET MEMS based probe along with an SS-OCT system. (A) *In vivo* human nail fold and (B) fingerprint images. Detailed tissue structures, such as the layered nail plate (NP), cuticle (C), stratum corneum (SC), stratum spinosum (SS), and sweat duct (SD) can be clearly identified. (C) *Ex vivo* rat intestine image; the submucosa (SM) layer can be identified between the mucosa (M) and muscularis propria (MP) layers. Scale bars: 500 μm.